Effect of Tungsten on the Pitting and Crevice Corrosion Resistance of Type 25Cr Super Duplex Stainless Steels

Eirik B. Haugan,[*] Monika Næss,[*] Cristian Torres Rodriguez,[*] Roy Johnsen,[*] and Mariano Iannuzzi[‡,*,**]

Submitted for publication: July 4, 2016. Revised and accepted: August 16, 2016. Preprint available online: August 16, 2016, http://dx.doi.org/10.5006/2185.

[‡]Corresponding author. E-mail: contact@aboutcorrosion.com.
[*]Norwegian University of Science and Technology (NTNU), Department of Engineering Design and Materials, Richard Birkelandsvei 2B, Trondheim 7091, Norway.
[**]General Electric Oil & Gas, Eyvind Lyches vei 10, P.O. Box 423, Sandvika 1339, Norway.

ABSTRACT

The oil and gas industry regularly uses Type 25Cr super duplex stainless steels (SDSS) for components exposed to seawater and hydrocarbon environments in topside facilities, downhole, and subsea equipment. Much debate still exists concerning the effect of tungsten on pitting and crevice corrosion resistance, particularly in standardization committees. Whereas some researchers claim that tungsten has a strong synergistic effect with molybdenum when added above a certain threshold value, others argue that tungsten additions at the expense of molybdenum could lower corrosion resistance. The objective of this investigation was to examine the effect of tungsten on localized corrosion of two super duplex stainless steels: a low-W (modified UNS S32750) and a high-W (UNS S39274) grade. Both crevice-free and creviced samples were studied. Tests were conducted in 3.5 wt% NaCl or natural seawater with temperatures ranging from 20°C to 95°C. Various independent methodologies including cyclic potentiodynamic polarization, electrochemical critical pitting temperature testing per ASTM G150, and long-term open-circuit potential exposure in natural seawater were used. Results showed that, in the solution annealed condition, tungsten additions to super duplex stainless steels had a marked positive effect on pitting and crevice corrosion resistance, increasing critical crevice temperatures by as much as 30°C. These findings suggested that tungsten-containing SDSS had a corrosion resistance on par with super austenitic stainless steel grades containing 6 wt% molybdenum. A new parametric definition of the pitting resistant equivalent is proposed to reflect the alloy's localized corrosion resistance and to support standardization efforts in the materials oil and gas community.

Key Words: critical crevice temperature, cyclic potentiodynamic polarization, oil and gas, seawater, super duplex stainless steels

INTRODUCTION

Duplex and super duplex stainless steels (DSS and SDSS, respectively) are steels composed of a two-phase ferritic-austenitic microstructure, the components of which are both stainless, i.e., they contain more than 10.5 wt% to 12 wt% chromium.[1-2] Although the ferrite content of DSS and SDSS can vary between 35 vol% and 55 vol%, manufacturers balance the steels close to the ideal 50-50 ferrite-to-austenite ratio.[1,3] DSS are ferritic-austenitic stainless steels with 22 wt% Cr and have a corrosion resistance on par with austenitic grades of similar Cr content.[1,3-5] Examples of DSS include UNS S32205(1) and UNS S31803. In contrast, SDSS are defined based not only on their chromium content but also on the alloy's pitting resistant equivalent (PRE).[4-5] In this regard, the PRE is an empirical formula that attempts to correlate the complex beneficial effect of the main alloying elements using a simple compositionally derived "pitting index."[6] While NORSOK M-001[4] defines PRE based on Cr, Mo, and N (Equation [1]),[4,7] ISO 21457[5] includes tungsten in the PRE expression (Equation [2]).

$$PRE_N = Cr + 3.3 \times Mo + 16 \times N \quad (1)$$

$$PRE_{N,W} = Cr + 3.3 \times (Mo + 0.5 \times W) + 16 \times N \quad (2)$$

In Equations (1) and (2), the sub-index "N" indicates that the original PRE expression suggested by Lorentz and Medawar[8] was modified to include nitrogen, while the sub-index "W" in Equation (2) shows that the PRE formula also includes tungsten.[9] In Equations (1) and (2), all values are given in wt%.

SDSS are, thus, defined as ferritic-austenitic stainless steels with 25 wt% Cr and a PRE ≥ 40.[4-5,7] The high Cr, Mo, and N content makes SDSS resistant to most oxidizing environments,[10-12] but are only considered seawater resistant by NORSOK M-001 and ISO 21457 up to 20°C because of crevice corrosion concerns.[13-14] The most common SDSS for subsea connection systems, piping, and tubing are UNS S32750, UNS S32550, and UNS S32760, which are all treated as equivalent[13] in NORSOK M-001,[4] NORSOK M-630,[7] and ISO 21457.[5] Table 1 summarizes the nominal composition of the most common DSS and SDSS used in oil and gas production.

DSS and SDSS combine high strength and localized and stress corrosion cracking (SCC) resistance at a competitive cost given the relatively small Ni content when compared to austenitic stainless steels.[3] Table 2 compares mechanical

(1) UNS numbers are listed in *Metals and Alloys in the Unified Numbering System*, published by the Society of Automotive Engineers (SAE International) and cosponsored by ASTM International.

properties of DSS and SDSS vs. selected austenitic stainless steels and nickel-based alloys to illustrate the advantages of DSS and SDSS over other alloys commonly used in the oil and gas industry.

At the time of this writing, there is much debate in the oil and gas community in Norway and in ISO standardization committees as to whether W, a ferrite stabilizer,[15] has a beneficial effect on localized corrosion resistance of SDSS. There is still no agreement on whether the PRE definition should include W in future revisions of the NORSOK M-001 specification.[4] Opponents to the inclusion of W and alignment with ISO 21457[5] argue that manufacturers could add W at the expense of Cr and Mo, creating some concerns regarding the seawater resistance of the resulting material. This reasoning, however, appears unjustified solely on a simple price comparison between the main alloying elements. W, a rare metal primarily used for high-temperature applications, is more expensive than both Cr and Mo;[16-18] tungsten additions are, therefore, intentional rather than a cost-saving strategy.

Although the effect of W on localized corrosion resistance has not been studied to the same extent as other alloying elements such as Cr, Mo, and N,[11] researchers agree that there exists an optimal W concentration; outside this range, W is either ineffective or detrimental.[19-20] Tomashov, et al.,[21] were the first to investigate the effect of W additions to an austenitic 18 wt% Cr-14 wt% Ni alloy. They reported that tungsten had a minor influence on localized corrosion resistance in 0.1 M NaCl at room temperature when compared to, e.g., Mo; however, tungsten had a net beneficial effect at around 3 wt%. Anh, et al., examined the influence of W and Mo on pitting potentials of laboratory-grade Fe-29 wt% Cr alloys.[22] The authors reported a linear relationship between pitting potentials (E_P) measured in 4 M $MgCl_2$ at 80°C and the alloy's W and Mo contents. When normalized to their corresponding atomic weights, the authors concluded that W and Mo increased E_P in almost the same amount.

Kim and Kwon[19] showed that a W-to-Mo weight ratio of 2 gave the best localized corrosion resistance. A W-to-Mo ratio of 2 contrasts, for example, with the W-to-Mo weight ratio of UNS S39274 and UNS S32760, which are approximately 0.70 and 0.25, respectively. Ogawa and coworkers[20] found a maximum in pitting corrosion resistance at 2 wt% W, both in the base metal and the heat affected zone (HAZ) of a welded SDSS, but with a W-to-Mo weight ratio of 0.72, in line with that of UNS S39274. Although the author did not specify the actual ratio in the article, Szklarska-Smialowska[23] mentions a particular W-to-Mo ratio in which a synergistic effect leads to peak corrosion performance.

Kim, et al., have analyzed the effect of tungsten additions to various austenitic and duplex laboratory-grade stainless steels, including Type 25Cr SDSS, on repassivation kinetics and SCC resistance in different environments.[24-25] Whereas Ni had a detrimental effect, results suggested that W additions to a 22.92 wt% Cr-6.18 wt% Ni-2.11 wt% Mo-0.07 wt% W (i.e., a W-to-Mo ratio of 0.033) and to a 17.92 wt% Cr-14.04 wt% Ni-2.05 wt% Mo-4.16 wt% W (i.e., a W-to-Mo ratio of 2.03) alloy improved repassivation kinetics as determined by the scratch test method in 1 M magnesium chloride ($MgCl_2$)

and 1 N sulfuric acid (H_2SO_4) + 3.5% Cl^-.[24] Tungsten in solid solution also seemed to improve SCC resistance noticeably in boiling 35% $MgCl_2$.[24-25]

It is still unclear whether W is enriched in the passive film as WO_3[26] or if dissolved W anions (i.e., tungstate, WO_4^{2-}) inhibit the electrolyte inside pits and crevices.[19,24-25,27] Bui and coworkers[26] studied the effect of tungsten additions to a base 16 wt% Cr-14 wt% Ni alloy, as well as the influence of dissolved tungstate. They concluded that both W additions to the base alloy and dissolved tungstate ions increased pitting potential and reduced the critical current for passivation in 0.2 M HCl. Additionally, the authors suggested that the direct formation of WO_3 at the surface in neutral NaCl solutions was responsible for the improved localized corrosion resistance. Kim, et al., proposed that W contributed to the stability of the passive film, leading to a decrease in the critical current density to reach passivation in simulated pit-like solutions, as well as to an increase in pitting potential in neutral NaCl electrolytes.[24] Kim, et al., attributed the improved passivity to a surface Mo accumulation in W-containing stainless steels, which was determined by auger emission spectroscopy.[24]

Independently of the effect of W in solid solution, researchers disagree about the possible retardation or acceleration of the precipitation kinetics of deleterious intermetallic compounds and tertiary phases during, e.g., welding operations. Ogawa, et al.,[20] Kim, et al.,[25] Kim and Kwon,[19] and, more recently, Park and Lee[28] studied the precipitation kinetics in DSS with and without W additions. The authors concluded that, during welding or isothermal heat treatments, W retards the formation of σ-phase for the less detrimental chi (χ)-phase and possibly Cr_2N in the HAZ. Ogawa, et al.,[20] showed that W additions above 2 wt% lowered impact toughness and localized corrosion resistance. Kim and Kwon[19] also investigated the effect of isothermal heat treatments at 850°C as a function of different W-to-Mo ratios. In accordance with Ogawa, et al.,[20] the authors reported that W retarded the formation of σ-phase, favoring χ-phase precipitation. A 3 wt% W-1.5 wt% Mo alloy showed the highest resistance to embrittlement induced by aging. This alloy also gave the best SCC resistance in boiling $MgCl_2$ and localized corrosion resistance to chloride-containing electrolytes.[19] Similarly, Park and Lee[28] found that substituting, in part, Mo with W retarded σ-phase precipitation in the HAZ. Tungsten-containing weldments had better pitting corrosion resistance than those containing exclusively Mo, with an optimal composition of 2.2 wt% Mo-2.2 wt% W.

Jeon, et al.,[27] recently studied the retardation of σ-phase precipitation when substituting Mo for W on a hyper-duplex stainless steel, i.e., a DSS with a $PRE_{N,W} \geq 50$. The authors reported that W strongly favored the precipitation of χ-phase, improving the overall pitting corrosion resistance. They supported their findings based on both thermodynamic modeling and experimental measurements. Moreover, the authors showed that adding W to the base alloy not only retarded σ-phase formation but also reduced the total volume fraction of tertiary phases.[27] The authors proposed that the preferential precipitation of the χ-phase during the early stages of aging depletes Mo and W along grain boundaries, reducing the driving force for σ-phase formation.[27] The main criticism to Jeon, et al., is that the authors focused on

relatively long, i.e., more than 600 s, temperature holding times, which are not representative of the temperature profiles experienced during welding.[29] A similar criticism can be made about the investigation by Kim and Kwon discussed earlier.

In clear contrast, work on Mo- and W-alloyed SDSS weld metals by Nilsson, et al.,[30] and computational simulations by Wessman and Pettersson[31] suggested that partial substitution of Mo by W caused a more rapid growth of intermetallic phases. Nilsson, et al.,[30] concluded that high-W (i.e., 2.16 wt% W) SDSS had a faster σ-phase precipitation kinetics than W-free and low-W counterparts. Likewise, Wessman and Pettersson[31] indicated that partial substitution of Ni by copper (Cu) appeared to retard σ-phase formation but could accelerate chromium nitride precipitation rates. In both studies, the investigators focused on short, i.e., less than 60 s, temperature holding times, which may better represent the transformations occurring during welding.[29]

Electrochemical Techniques in Localized Corrosion Research

Electrochemical techniques are valuable tools to quantify the effect of microstructure on localized corrosion performance.[32] Anodic cyclic potentiodynamic polarization (CPP) testing can be used to evaluate the pitting and crevice corrosion behavior of an alloy under various metallurgical conditions.[12,33] During CPP, the working electrode is first scanned forward in the anodic direction at a given scan rate and reverted once the current reaches a certain value.[34] For most stainless steels in halide solutions, CPP provides two main parameters: (i) the pitting potential E_P (or crevice potential, E_{Crev}, if using creviced samples) and (ii) the repassivation potential E_{RP} (or $E_{RP,Crev}$ if using creviced specimens).[35] Whereas E_P is a measure of the alloy's resistance to pit initiation, E_{RP} has been shown to correlate well with the alloy's overall resistance to localized corrosion.[36] Dunn, et al.,[34] and Sridhar and Cragnolino[36] suggested that, above a certain critical charge density value, E_{RP} becomes independent of the current density at scan reversal. For UNS S31600 and UNS N08825, E_{RP} became independent of prior pit growth for deep pits. In this regard, deep pits were associated with a critical charge density of 10 C/cm^2.[36] Therefore, the authors concluded E_{RP} could be used as a reliable estimator of localized corrosion resistance when the charge density criterion is met. E_{RP} has also been used in parametric models to predict long-term corrosion performance.[34,36-37]

While some studies have investigated the corrosion behavior of SDSS as a function of W content using various electrochemical and immersion techniques, the effects of W on repassivation kinetics, crevice corrosion initiation, and long-term performance remain unclear. The objective of this investigation was to compare the localized corrosion resistance of two SDSS: (i) a conventional low-W grade (i.e., a modified UNS S32750) and (ii) a commercial high-W SDSS (i.e., UNS S39274). The scope of the work was to establish the critical pitting temperature (CPT) and the critical crevice temperature (CCT) using CPP testing, temperature ramping at a fixed anodic potential, and long-term open-circuit potential (OCP) exposure in natural seawater.

EXPERIMENTAL PROCEDURES

Materials

Samples were cut from (i) a low-W modified UNS S32750 forged bar with an outer diameter of 30 mm, taken from an actual production run used to manufacture blind dowel pins and (ii) a 100 mm by 150 mm by 9.5 mm UNS S39274 plate. Both materials were tested in the solution annealed (SA) condition. The UNS S32750 bar was SA for 30 min at 1,100°C, followed by water quenching. UNS S39274 was solution annealed at 1,110°C for 600 s and water quenched. Table 3 summarizes actual chemical compositions and both the PRE_N and $PRE_{N,W}$ of the two materials.

For both crevice-free and creviced tests, samples were cut into 3-mm-thick disks that were 30 mm in diameter and had an average surface area of 16.9 cm^2. A small, 2 mm hole drilled close to the perimeter of the samples served as the sample holder. The test specimens were suspended using a 200 µm platinum wire that acted as an electric connection.

Sample Preparation

Samples were polished down to 600 grit SiC paper using ethanol as a lubricant. Samples were subsequently rinsed in acetone, deionized (DI) water, and ethanol and cleaned in an ultrasonic bath for 300 s.

A subset of samples was pickled according to NORSOK M-630 recommendations.[7] Test coupons were immersed in a solution of 20% nitric acid (HNO_3) and 5% hydrofluoric acid (HF) at 60°C for 300 s, followed by a thorough DI-water rinse. Special safety procedures for handling HF were followed. All samples were stored in a desiccator for 24 h before testing, which is often referred to as "passivation."[7,38]

Cyclic Potentiodynamic Polarization Testing

CPP testing was conducted on crevice-free and creviced specimens in accordance with ASTM G61.[35] For creviced samples, a spring-loaded crevice assembly was used.[39] Flat polytetrafluoroethylene (PTFE) crevice formers were used as described by Steinsmo, et al.,[40-41] and Høydal, et al.[42] The titanium bolt was electrically isolated using a heat-shrinkable tube. The crevice assembly was mounted using a torque of 2 N·m. More details can be found elsewhere.[42]

A deaerated 3.5 wt% NaCl (0.62 M NaCl) pH 8.0 solution was used as electrolyte. The solution pH was left unadjusted and monitored before and after testing. Tests were conducted at eight different temperatures: 25, 30, 40, 50, 60, 70, 80, and 90°C. The temperature was controlled using a regulating hot plate. The actual solution temperature was continuously monitored during testing and kept within ±1°C.

Cyclic anodic polarization curves were obtained using a conventional three-electrode array. A saturated calomel electrode (SCE) was used as reference electrode. The reference electrode was placed in a separate compartment kept at room temperature and connected to the electrochemical cell using a salt bridge. The test solution was purged for 1 h using high-purity nitrogen gas before immersing the samples in the solution. Nitrogen purging was maintained for the

duration of the anodic polarization. Upon immersion, samples were left at the corrosion potential (E_{corr}) for 1 h before polarization. Samples were subsequently polarized in the anodic direction at a scan rate of 600 mV/h (0.167 mV/s). Scan reversal occurred once the current density reached 5 mA/cm^2. The test was completed when the hysteresis loop closed or upon reaching OCP.

ASTM G150—Electrochemical Critical Pitting Temperature

A subset of crevice-free UNS S32750 and UNS S39274 specimens was used to determine the potential independent CPT using a complimentary approach as described in ASTM G150.[43] Samples were polished to 600 grit paper, pickled, and passivated as outlined in the *Materials* section. Tests were performed in 3.5 wt% NaCl with a pH = 8.0. Samples were polarized to an applied potential, E_{App}, of 600 mV_{SCE} for 5 min before and during temperature ramping. The solution temperature was ramped at a rate of 1°C/min from 20°C to 95°C, or until a maximum current density of 150 µA/cm^2 was reached, whichever occurred first. The CPT was determined as the temperature at which i = 100 µA/cm^2.[43]

Long-Term Open-Circuit Exposure

Creviced UNS S32750 and UNS S39274 specimens, prepared using the method described by Kivisäkk and Novak,[39] Steinsmo, et al.,[40-41] and Høydal, et al.,[42] were exposed to filtered natural seawater obtained directly from the Trondheim fjord at NTNU's seawater laboratory. The main advantage of the spring-loaded crevice assemblies used herein is that no significant drop in applied force has been observed even after long-term testing at elevated temperatures.[39]

The initial temperature was set to 60°C, which was above the CCT determined by CPP for UNS S32750. A temperature of 60°C was also shown to be an adequate choice for SDSS by Johnsen and Vingsand.[44-45] Both temperature and E_{corr} were monitored during exposure. If no drop in E_{corr} was observed after 750 h, the temperature was increased to 70°C and kept at that temperature for another 400 h or until a sudden decrease in E_{corr} was detected, whichever occurred first. If no drop in E_{corr} was measured after a total exposure time of 1,150 h, then the temperature was increased to 80°C. This process was repeated until crevice corrosion initiation occurred. More details about the experimental setup can be consulted elsewhere.[40,44-45]

Characterization

A group of samples was first polished and etched following ASTM A923 recommendations to determine the absence of deleterious phases before testing.[46] Test specimens were etched in a 40 wt% sodium hydroxide (NaOH) solution using 1.5 V for 30 s to 40 s. After etching, the test coupons were rinsed in acetone followed by air drying. Samples were then examined using confocal and scanning electron microscopes.

After testing, samples were rinsed in DI-water and stored in a desiccator. Samples were analyzed in the optical microscope to determine the presence of pits and the absence of crevice attack at the connection point. Samples were

gently cleaned using a 3-µm diamond suspension to remove corrosion products and to reveal sub-surface pits.[11] Creviced samples exposed at E_{corr} were also analyzed with the scanning electron microscope.

Reproducibility and Characterization

All tests were conducted in duplicate or triplicate to verify reproducibility. Figures and tables show either all of the data points or average values, as indicated.

RESULTS

Materials Characterization

Figures 1 and 2 show both optical and secondary electron images of as-received and etched SA UNS S3270 and UNS S39274, respectively. Whereas UNS S32750 had an equiaxed fine grain structure, characteristic of forged products, UNS S39274 had elongated grains aligned in the rolling direction, typical of rolled plates.[46] Both alloys had mechanical properties that exceeded the minimum requirements of ASTM A182[47] and NORSOK M-630[7] standards, as well as UNS S32750 and UNS S39274 specifications (Table 4).

Charpy V-notch (CVN) and ASTM G48 method A[48] results, as well as optical microscopy, suggested that the material was free of deleterious phases. The volume fraction of austenite was 47 vol%, whereas the volume fraction of ferrite was 53 vol%, as determined by optical microscopy in accordance with ASTM A923[46] and ferritescope.

Differences in microstructure introduced by the manufacturing process could affect corrosion performance,[1,10-11,15,40,49-50] in particular, resistance to hydrogen stress cracking.[51-52] Nevertheless, in this work, the localized corrosion resistance was assumed to be primarily controlled by alloy composition, in line with, e.g., the work by Sendriks and Newman.[10-11] This hypothesis is justified based on the adequate average austenite and ferrite volume fractions, which were close to the ideal 50% in both cases,[1,3] the lack of deleterious intermetallic compounds and tertiary phases evidenced by optical and scanning electron microscopy (Figures 1 and 2), as well as ASTM G48 method A quality control testing.

Anodic Polarizations

The shape of the anodic polarization curves depended on the composition, the microstructure of the test specimen, the type of coupon (i.e., crevice-free or creviced), and the temperature of the solution. Nevertheless, all polarization plots could be grouped into three distinct cases: (i) curves showing no hysteresis, (ii) curves showing high E_P or E_{Crev} if using crevice formers and little hysteresis, and (iii) curves showing large positive hysteresis loops. Figure 3 illustrates the three cases. The inflection seen in curves showing no hysteresis or high E_P or E_{Crev} and little hysteresis was, primarily, associated with the oxygen evolution reaction caused by water oxidation and transpassive dissolution at the transpassive potential, E_{Trans}.[11,53-55] The presence of small pits concurrent with oxygen evolution translated into small hysteresis loops. Given that the total current is the sum of pit propagation and water oxidation, it was not possible to

discern whether the 10 C/cm^2 critical charge density criterion proposed by Dunn, et al.,[34] was met in those cases. In contrast, curves displaying significant positive hysteresis loops were always associated with pitting or crevice, if using crevice formers, corrosion.

Although pitting corrosion was accompanied by uniform dissolution, especially at higher temperatures, it is reasonable to assume that, for crevice-free samples, most of the current was associated with pitting corrosion. Integration of the current density vs. time curve confirmed that the deep pit condition was exceeded in all cases. Thus, E_{RP} values corresponded to a lower-bound critical potential that could be used to estimate the conditions for crevice corrosion initiation.[34,36-37]

To be consistent with Sridhar and Cragnolino,[36] E_P was determined at the inflection point of the E vs. i plot, while E_{RP} values were identified as the potential, in the backward scan, where the current density reached 2 μA/cm^2. Likewise, the passive current density, i_{pass}, was measured as the mean current density in the passive region. A similar approach was followed to determine E_{Crev} and $E_{RP,Crev}$ for creviced specimens.

Critical Pitting Temperature, Protection Temperature, and Critical Crevice Temperature Based on Cyclic Potentiodynamic Polarization Testing

Crevice-Free Samples—

CPT values were obtained at the inflection point of E_{Trans} or E_P vs. temperature diagrams. The CPT was calculated as the mean temperature between the temperature of the last E_{Trans} and the first E_P potential. Because the temperature step was 10°C, there was an average ±5°C margin of error. Similarly, the protection temperature (T_{Prot}) was taken at the inflection point of E_{Trans} or E_{RP} vs. temperature curves, calculated following the same procedure. Figure 4 illustrates E_{Trans}, E_P, and E_{RP} vs. temperature maps for UNS S39274, whereas Figure 5 compares average E_{Trans} or E_{RP} potentials as a function of temperature for UNS S32750 and UNS S39274. CPT and T_{Prot} values are summarized in Table 5.

Whereas the CPT of UNS S32750 was 65°C to 75°C for the as-polished condition and 75°C for pickled surfaces, the CPT of UNS S39274 was 85°C regardless of surface condition. There was some degree of uncertainty in establishing CPT for as-polished samples, as the transition was more gradual than in the other cases. Tests in the 60°C to 75°C range using a smaller temperature interval could give a better approximation. Likewise, the mean T_{Prot} of UNS S32750 was 55°C, whereas that of UNS S39274 was approximately 85°C. Because, for any given test condition, the potential dropped from the transpassive region to measurable E_P or E_{RP} values at the same temperature, min. and max. CPT and T_{Prot} results shown in Table 5 were identical. The only exception was the CPT of UNS S32750 in the polished and passivated case, where the drop in critical potential occurred at different temperatures.

No clear differences were observed between polished and passivated and pickled and passivated samples. Nevertheless, pickled and passivated surfaces led to less scatter. A more detailed discussion on the differences between the two surface preparation methods is presented elsewhere.[56]

Creviced Samples—

To verify the validity of CCT values estimated using T_{Prot} on crevice-free specimens, i.e., CCT|E_{RP}, CPP was also conducted on creviced coupons. Given the small difference in E_P and E_{RP} between as-polished and passivated and pickled and passivated samples, which was in line with the findings discussed by Szklarska-Smialowska[23] and DeForce,[57] the remaining tests were performed on polished and passivated samples only.

There was no clear inflection in E_{Crev} as a function of temperature. Therefore, no reliable CCT could be inferred from E_{Trans} or E_{Crev} vs. temperature diagrams (Figure 6[a]). Nonetheless, a clear inflection point was observed in the crevice repassivation, $E_{RP,Crev}$, vs. temperature curves (Figure 6[b]). As shown in Table 6, the average critical crevice repassivation temperature (CCRT) of UNS S39274 was 11°C higher than that of UNS S32750, i.e., 67.5°C vs. 56.5°C.

Electrochemical Critical Pitting Temperature as per ASTM G150

The CPT of UNS S32750 and UNS S39274 was independently determined on crevice-free samples using the potentiostatic test method described in ASTM G150.[43] As seen in Figure 7, whereas UNS S32750 suffered pitting corrosion at 63.5°C to 65.5°C, the CPT of UNS S39274 exceeded 95°C. The E_{App} = 600 mV_{SCE} value was chosen to simulate the potential reached in chlorinated seawater systems with 0.5 ppmw residual chlorine.[40,58-59] A similar potential was used by Johnsen and Vingsand to study the long-term crevice corrosion resistance of SDSS, including UNS S32750, and nickel-based alloys.[44-45]

Long-Term Open-Circuit Potential Exposure in Natural Seawater

Figure 8 compares E_{corr} vs. time plots of creviced UNS S32750 and UNS S39274 specimens, respectively. The temperature increase profile is overlapped in the figures. Photomicrographs are also included to illustrate the presence of crevice corrosion after testing, which nucleated at the periphery of the crevice former in all cases. In Figure 8, a sudden drop in E_{corr} from values reflecting a passive state to active, i.e., negative, potentials determines the initiation of crevice attack. As shown by Newman and Galvele,[10,60] the crevice (or pitting) potential of the material controls the sharp decrease in E_{corr} observed during long-term OCP exposure.

UNS S32750 suffered crevice corrosion at 60°C and tests were stopped with no further temperature rise. The induction time, i.e., the time for crevice corrosion initiation,[53] varied between 416 h and 656 h. In contrast, UNS S39274 did not suffer crevice corrosion up to 80°C. Samples were exposed for a total of 1,416 h to 1,626 h before crevice corrosion initiation. The induction time at 80°C was between 312 h and 520 h.

Figure 9 shows the morphology and the extent of the crevice corrosion attack after long-term OCP exposure in natural seawater. As seen in Figure 9, UNS S32750 suffered selective dissolution of the austenite phase, which was later confirmed by EDS analysis. In contrast, the high-W UNS S39274 grade did not present clear evidence of selective phase dissolution. Additionally, the depth of the crevice corrosion attack observed in UNS S39274 specimens was shallower on average than in UNS S32750. Selective phase dissolution is common in DSS.[61-62] The preferential attack depends primarily on the partitioning of alloying elements to austenite or ferrite,[61,63-64] which in turn defines the critical localized corrosion potential of the phase (and the local PRE).[65] The phase with the lowest critical localized corrosion potential dissolves first and determines the alloy's overall pitting or crevice potentials.[1,10,60-61,63,65]

DISCUSSION

The CPT of UNS S32750 as determined by CPP testing was 5°C to 15°C lower and 15°C to 17°C lower than CPT values reported by the alloy manufacturer[66-67] in 6 wt% and 10 wt% $FeCl_3$, respectively. Measured CPT values were also 10°C to 32°C lower than CPT values reported by the alloy manufacturer obtained by ASTM G150 testing in 1 M NaCl (Table 2). Likewise, CPT values found by CPP and ASTM G150 testing at 600 mV_{SCE} were 12°C to 22°C and 22°C to 24°C lower, respectively, than results reported by Deng, et al.[68] Deng and coworkers determined a mean CPT of 87.6±0.4°C for UNS S32750 using temperature ramping at a constant applied potential of 750 mV_{SCE} in 1 M NaCl. CPT values obtained by ASTM G61 testing were, however, in close agreement with Steinsmo, et al.,[40] for the same alloy, but evaluated potentiostatically in seawater at 600 $mV_{Ag/AgCl}$. The authors reported CPT values for SA UNS S32750 of 76°C,[40] which was just 1°C higher than the CPT obtained by CPP, but between 10°C and 13°C higher than those measured herein as per ASTM G150.[67] ASTM G61 results were, too, in agreement with Tsaprailis, et al.[69] Tsaprailis and coworkers obtained a CPT = 71°C for UNS S32750 in 10 wt% $FeCl_3$, determined using zero resistance amperometry (ZRA) at a temperature scan rate of 0.5°C/min. This value was 6°C to 8°C higher than the CPT values obtained herein as per ASTM G150.[67]

UNS S39274 had a CPT as determined by CPP and ASTM G150 that was between 15°C and 20°C and between 20°C and >30°C, respectively, higher than that of UNS S32750 depending on surface condition and test method. It is also remarkable that one of the specimens did not suffer pitting corrosion during the potentiostatic hold at 600 mV_{SCE} exposure even after reaching the boiling point. These results lie within the experimental error reported by Kim and Kwon.[19] Results were also in close agreement with Ogawa, et al.[20] Ogawa, et al.,[20] measured CPT as a function of W content in a 10 wt% $FeCl_3$ solution at the OCP. Ogawa reported a CPT of at least 80°C for 25 wt% Cr-7 wt% Ni-3 wt% Mo samples containing between 2 wt% and 4.5 wt% W. Ogawa, et al., suggested that the CPT of samples with more than 2 wt% W exceeded the highest temperature used in their investigation, which was close the acceptable temperature limit for testing in a 6 wt% to 10 wt% $FeCl_3$ electrolyte.[48,70]

In addition to W, the two materials used in this investigation also differed in their Cu content. The modified UNS S32750 alloy had a Cu content that was about 60% lower than that of UNS S39274. Researchers have found that Cu additions to

SDSS increase pitting potential and overall localized corrosion resistance to halide environments.[61,64] It may be questioned, therefore, whether the difference in Cu could be responsible for the outstanding resistance of UNS S39274. Garfias-Mesias and Sykes[64] and Garfias-Mesias, et al.,[61] conducted extensive investigations on Cu-modified SDSS using a variety of electrolytes and electrochemical techniques. The authors have shown that the extent to which Cu improves localized corrosion resistance strongly depends on the partitioning of the main alloying elements during solution annealing. However, the highest CPT measured for a 25.92 wt% Cr-3.19 wt% Mo-0.20 wt% N-1.62 wt% Cu (PRE_N = 39.65) was 64°C, much lower than the 85°C of UNS S39274. A low-Cu alloy with a PRE_N = 40.23 wt% and 0.56 wt% Cu had a CPT of 61.8°C. Therefore, it seems reasonable to assume that the difference in localized corrosion performance should be attributed primarily to W.

The Repassivation Potential as an Estimator of Crevice Corrosion Resistance

According to Sridhar and Cragnolino,[36] E_{RP} becomes independent of prior pit growth only above a certain pit depth. In line with the interpretation first given by Galvele in his seminal publication on localized corrosion,[71] a growing pit can be visualized as a particular form of crevice corrosion.[33-34,36-37] Nevertheless, it is worth mentioning that, for stainless steels, some researchers argue this may be an over-simplistic interpretation.[72] Using Galvele's analogy, the E_{RP} indirectly estimates the ease with which a crevice can grow stable.[60] Given that the deep pit condition was met or exceeded above the inflection point in E_{RP} vs. temperature curves, T_{Prot} was used as an estimator of the CCT. Although E_{RP} and T_{Prot} cannot provide mechanistic information regarding crevice corrosion kinetics, both parameters relate to conditions leading to crevice corrosion initiation.[33-34,36] CCT values indirectly estimated by E_{RP} (i.e., CCT|E_{RP}) vs. temperature curves were 15°C to 25°C lower than the CPT of UNS S32750 and independent of surface finish. In contrast, the CCT|E_{RP} of UNS S39274 was virtually identical to CPT and 25°C to 30°C higher than that of UNS S32750, suggesting W favored pit repassivation kinetics as proposed by Bui, et al.,[26] and Lumsden and Szklarska-Smialowska[73] (Figure 5). The effect of W on facilitating repassivation was also evidenced by the difference in CCRT between UNS S39274 and UNS S32750, shown in Figure 6.

CCT|E_{RP} values of UNS S32750 were almost 25°C lower than values reported by Deng, et al.,[68] using cyclic temperature ramping at an applied potential of 750 mV_{SCE} in 1 M NaCl, but 5°C higher than reported CCT values obtained by conventional ASTM G48 method D.[48] Nevertheless, results were in reasonable agreement with CCTs reported by Høydal, et al.[42] Høydal and coworkers investigated crevice corrosion of UNS S32760 as a function of temperature using flat PTFE rods as crevice formers. UNS S32760 is an SDSS grade that, although it is equivalent to UNS S32750 according to NORSOK M630,[7] contains W and Cu (Table 1). A comparison between Tables 1 and 3 reveal that the modified UNS S32750 composition used in this investigation had a W content similar to that of UNS S32760, but a lower Cu amount. Høydal, et al.,[42] polarized all samples potentiostatically at various anodic potentials while increasing the temperature 4°C/d. The authors reported CCT values of 51±1°C at 600 $mV_{Ag/AgCl}$ and between 61°C and 63°C for potentials in the 500

$mV_{Ag/AgCl}$ to 550 $mV_{Ag/AgCl}$ range. Similarly, results were in close agreement with Francis, et al.,[59] who reported a CCT of approximately 55°C for UNS S32760 in seawater at 600 $mV_{Ag/AgCl}$.

Results from the long-term OCP exposure testing on creviced UNS S32750 samples shown in Figure 8 were consistent with Johnsen and Vingsand.[44-45] The authors investigated crevice corrosion of UNS S32750 and two nickel-based alloys in conditions that simulated chlorinated seawater exposure. The authors reported crevice corrosion of UNS S32750 at 60°C, suggesting that crevice corrosion could initiate between 50°C and 60°C.[44-45] Likewise, Johnsen and Vingsand showed that crevice corrosion started close to the edge of the crevice former, which matched the type of attack presented in Figures 8 and 9. Nevertheless, no clear preferential phase dissolution was shown by the investigators. Results were also in line with Høydal, et al., and Francis and collaborators.[42,59]

Before this work, there has been no CCT and long-term performance data for UNS S39274 reported in the open literature. This work suggested that CCT|E_{RP} determined by CPP testing and by results of long-term OCP exposure were in agreement with CCT documented by a UNS S39274 manufacturer.[74] In their report, the CCT was determined in aerated NaCl solutions with a variable chloride content. The authors described CCT values of approximately 80°C, which were comparable with the CCT of UNS S31254, a Type 6Mo super austenitic stainless steel with a PRE_N of about 43.3.[75] The current work represents the first independent confirmation of the manufacturer's crevice corrosion resistance claims. The outcome of long-term testing is also supported by a 430-d exposure testing in various natural and chlorinated Arabian seawater compositions done by Malik, et al.[76] The authors found that UNS S39274 outperformed both UNS S31254 and UNS S32750 in all test conditions.

Differences in CCT|E_{RP} and CCT are difficult to examine given that crevice geometry and, for practices using crevice formers, the material utilized for the multi-crevice assembly (e.g., PTFE, ceramic, or PTFE-covered ceramic) and torque strongly affect crevice corrosion results.[77] Nevertheless, it is interesting to highlight the close agreement between critical crevice temperatures indirectly estimated by T_{Prot}, i.e., CCT|E_{RP}, and the crevice corrosion resistance observed in long-term OCP exposure. Thus, E_{RP}, as determined by CPP testing on coupons without crevice formers, was a good estimator of crevice corrosion resistance. These findings are also in line with the recent work by Kappes, et al.,[78] and Martinez and collaborators[79] on SDSS. The researchers have found excellent agreement between tests conducted using crevice-free specimens exposed to simulated crevice-like solutions following Galvele's approach[71,80] and results of potentiodynamic-galvanostatic-potentiodynamic (PD-GS-PD) testing on creviced coupons.

Despite its potential, the use of E_{RP} to gauge crevice corrosion resistance has limitations. For cases where only little hysteresis is observed and when pitting is concurrent with oxygen evolution and transpassive dissolution, the system may not meet the deep pit condition (Figure 3[b]). Therefore, E_{RP} values, as determined by ASTM G61 testing,[35] cannot be used to establish immunity to localized corrosion. Alternative electrochemical techniques such as the PD-GS-PD and

potentiodynamic-potentiostatically-potentiodynamic (PD-PS-PD)[78-79,81] methods and ZRA[63,69,82] could give valuable information about the influence of test conditions on CPT and CCT.

A Parametric Pitting Resistant Equivalent Definition

UNS S39274 CPT and CCT values were higher than those of UNS S32750 by as much as 30°C (Figures 5, 7, and 8). CPT and CCT values were, in fact, comparable to those of super austenitic stainless steels with a PRE_N above 43. Yet, UNS S39274 has a specified minimum yield strength (SMYS) that almost doubles that of UNS S31254. The results presented herein suggest that W in solid solution plays a decisive role in increasing localized corrosion resistance when added to SDSS at about 2.2 wt%. Moreover, the higher CCRT measured by CPP on creviced samples also suggested that W additions led to a faster repassivation kinetics than that of low-W or W-free SDSS, results that are in line with the effect of W additions to Ni-based alloys.[83-85] Adding W to the PRE formula as detailed by ISO 21457[5] translates to a $PRE_{N,W}$ of 43.87 (Table 3), similar to that of super austenitic stainless steel grades containing 6 wt% Mo (e.g., UNS S31254).[75]

The results of this investigation clearly indicated that UNS S39274 has a localized corrosion resistance equivalent to that of stainless steels containing higher amounts of Cr and Mo. It seems reasonable, thus, to postulate a PRE expression that better reflects the actual performance of the alloy and separates UNS S39274 from conventional Type 25Cr SDSS. A parametric definition of PRE is proposed that could replace the current NORSOK M-001[4] and ISO 21457[5] PRE formula (Equation [3]). As shown in Equation (3), tungsten is introduced with a multiplying factor as detailed in ISO 21457[5] only when W is added within the limits established by, e.g., ASTM A182[47] for UNS S39274, which is in line with Ogawa, et al. Likewise, the authors propose to maintain $PRE_N = 40$ as the seawater resistance threshold to avoid the discussion on whether W is added at the expense of Cr or Mo on SDSS with a W content $\leq$ 1.5 wt% . It is important to emphasize that the parametric PRE definition proposed herein exclusively applies to SDSS. In Ni-based alloys, where the beneficial effects of W have been broadly recognized,[83-85] there shall be no limitation on the W content allowed in the $PRE_{N,W}$ equation.

If 1.5 wt% ≤ W ≤ 2.5 wt%:

$$PRE_{N,W} = Cr + 3.3 \times (Mo + 0.5 \times W) + 16 \times N$$

Otherwise:

$$PRE_N = Cr + 3.3 \times Mo + 16 \times N \qquad (3)$$

More research is still needed to determine the actual W multiplier, e.g., 0.5 as proposed in ISO 21457 or 1.0 as suggested early on,[6,23,53] in the PRE formula and whether W affects the precipitation kinetics of deleterious phases during welding. However, precipitation kinetics effects shall not influence the PRE formula used in international standards, as the bulk PRE is insensitive to local compositional changes occurring during the precipitation of deleterious

phases. The actual mechanisms by which tungsten improves localized corrosion resistance remain unclear to date, but results presented herein point to a strong effect on repassivation kinetics.

CONCLUSIONS

In this work, the effect of W on localized corrosion resistance was investigated by comparing two commercial SDSS chemistries: a low-W modified UNS S32750 and a high W-containing UNS S39274. The following conclusions were drawn based on the evidence presented herein:

- When added at about 2.2 wt%, W had a marked beneficial effect on pitting and repassivation potentials, as well as pitting and crevice repassivation kinetics.
- In the solution annealed condition, the CCT as determined by various independent techniques was up to 30°C higher for UNS S39274 than for UNS S32750.
- CCT values as estimated by E_{RP} were in reasonable accord with results of long-term OCP exposure and literature ASTM G48 method D results, suggesting that E_{RP} measured using coupons without crevice formers could be used to the estimate crevice corrosion resistance of SDSS.
- Based on the evidence presented herein, it seems reasonable to accept the inclusion of W in the NORSOK M-001 and ISO 21457 PRE formula with a multiplying factor as detailed in ISO 21457 when W is added in the 1.5 wt% to 2.5 wt% range, maintaining a $PRE_N = 40$ as seawater resistance threshold for SDSS.

ACKNOWLEDGMENTS

We thank Atle H. Qvale (GE O&G), Alexander Fjeldly (GE O&G), Leif Brattås (GE O&G), Anders Wiktorsson (GE O&G), and Mariano A. Kappes and Ricardo M. Carranza (Instituto Sabato, Buenos Aires, Argentina) for their guidance, support, and technical discussions.

This work was funded by General Electric, Co. (Oil and Gas, Norway) and conducted at NTNU's Department of Engineering Design and Materials (IPM).

References

1. J. Charles, "Super Duplex Stainless Steels: Structure and Properties," Duplex Stainless Steels '91 (Beaune, France: Les Éditions de Physique, 1991), p. 151-168.
2. G. Krauss, "Stainless Steels,"in *Steels: Processing, Structure, and Performance* (Materials Park, OH: ASM International, 2005), p. 495-534.

3. J.O. Nilsson, *Mater. Sci. Technol.* 8, 8 (1992): p. 685-700.

4. NORSOK M-001, "Materials Selection" (Lysaker, Norway: Standards Norway, 2014).

5. ISO 21457:2010, "Petroleum, Petrochemical and Natural Gas Industries – Materials Selection and Corrosion Control for Oil and Gas Production Systems" (Geneva, Switzerland: International Organization for Standardization, 2010).

6. R.F.A. Jargelius-Pettersson, *Corrosion* 54, 2 (1998): p. 162-168.

7. NORSOK M-630, "Material Data Sheets and Element Data Sheets for Piping" (Lysaker, Norway: Standards Norway, 2013).

8. K. Lorentz, G. Medawar, *Tyssenforschung* 1, 3 (1969): p. 97-108.

9. A.U. Malik, N.A. Siddiqi, S. Ahmad, I.N. Andijani, *Corros. Sci.* 37, 10 (1995): p. 1521-1535.

10. R.C. Newman, *Corrosion* 57, 12 (2001): p. 1030-1041.

11. A.J. Sedriks, *Corrosion* 42, 7 (1986): p. 376-389.

12. R. Sriram, D. Tromans, *Corrosion* 45, 10 (1989): p. 804-810.

13. J.I. Skar, S. Olsen, "Development of the NORSOK M-001 and ISO 21457 Standards – Basis for Defining Materials Application Limits," CORROSION 2016, paper no. 7433 (Houston, TX: NACE International, 2016).

14. G. Byrne, R. Francis, G. Warburton, M. Maligas, "The Selection Of Superduplex Stainless Steel For Oilfield Applications," CORROSION 2004, paper no. 123 (Houston, TX: NACE, 2004).

15. J.E. Truman, "Stainless Steels,"in *Materials Science and Technology* (Hoboken, NJ: John Wiley & Sons, 2006), p. 529-581.

16. "Alfa Aesar: Molybdenum Rod," Fisher Scientific, 2016, https://goo.gl/9OKfnb.

17. "Alfa Aesar: Tungsten Rod," Fisher Scientific, 2016, https://goo.gl/idMjtG.

18. "Alfa Aesar: Chromium Rod," Alfa Aesar, 2016, https://goo.gl/t4tcAs.

19. J.S. Kim, H.S. Kwon, *Corrosion* 55, 5 (1999): p. 512-521.

20. K. Ogawa, H. Okamoto, M. Ueda, M. Igarashi, T. Mori, T. Kobayashi, *Weld. Int.* 10, 6 (1996): p. 466-472.

21. N.D. Tomashov, G.P. Chernova, O.N. Marcova, *Corrosion* 20, 5 (1964): p. 166t-173t.

22. M.K. Ahn, H.S. Kwon, H.M. Lee, *Corros. Sci.* 40, 2-3 (1998): p. 307-322.

23. Z. Szklarska-Smialowska, "Surface Treatments," in *Pitting and Crevice Corrosion* (Houston, TX: NACE, 2005), p. 519-533.

24. J.S. Kim, P.J. Xiang, K.Y. Kim, *Corrosion* 61, 2 (2005): p. 174-183.

25. K.Y. Kim, P.Q. Zhang, T.H. Ha, Y.H. Lee, *Corrosion* 54, 11 (1998): p. 910-921.

26. N. Bui, A. Irhzo, F. Dabosi, Y. Limouzin-Maire, *Corrosion* 39, 12 (1983): p. 491-496.

27. S.-H. Jeon, S.-T. Kim, I.-S. Lee, J.-S. Kim, K.-T. Kim, Y.-S. Park, *J. Alloys Compd.* 544 (2012): p. 166-172.

28. H.J. Park, H.W. Lee, *Int. J. Electrochem. Sci.* 9, 12 (2014): p. 6687-6698.

29. J.C. Lippold, D.J. Kotecki, "Duplex Stainless Steels," in *Welding Metallurgy and Weldability of Stainless Steels* (Hoboken, NJ: John Wiley & Sons, 2005), p. 230-245.

30. J.O. Nilsson, P. Kangas, A. Wilson, T. Karlsson, *Metall. Mater. Trans. A* 31, 1 (2000): p. 35-45.

31. S. Wessman, R. Pettersson, *Steel Res. Int.* 86, 11 (2015): p. 1339-1349.

32. P.E. Manning, *Corrosion* 39, 3 (1983): p. 98-102.

33. B.E. Wilde, E. Williams, *Electrochim. Acta* 16, 11 (1971): p. 1971-1985.

34. D.S. Dunn, G.A. Cragnolino, N. Sridhar, *Corrosion* 56, 1 (2000): p. 90-104.

35. ASTM G61-86(2014), "Standard Test Method for Conducting Cyclic Potentiodynamic Polarization Measurements for Localized Corrosion Susceptibility of Iron-, Nickel-, or Cobalt-Based Alloys" (West Conshohocken, PA: ASTM International, 2014).

36. N. Sridhar, G.A. Cragnolino, *Corrosion* 49, 11 (1993): p. 885-894.

37. N. Sridhar, C.S. Brossia, D.S. Dunn, A. Anderko, *Corrosion* 60, 10 (2004): p. 915-936.

38. GS EP PVV 619, "General Specification - Piping Valves Vessels: Piping or Pressure Vessel Components in Duplex and Superduplex Stainless Steel" (Paris, France: Total, 2006).

39. U. Kivisäkk, P. Novak, "Qualification Testing of Superduplex Stainless Steel Tubing for Umbilicals," CORROSION 2005, paper no. 228 (Houston, TX: NACE, 2005).

40. U. Steinsmo, T. Rogne, J. Drugli, *Corrosion* 53, 12 (1997): p. 955-964.

41. U. Steinsmo, T. Rogne, J.M. Drugli, P.O. Gartland, *Corrosion* 53, 1 (1997): p. 26-32.

42. A.B. Høydal, E. Skavås, T. Hemmingsen, "Crevice Corrosion on Super Duplex Stainless Steel – Effect of Potential on Critical Crevice Corrosion Temperature," CORROSION 2013, paper no. 2763 (Houston, TX: NACE, 2013).

43. ASTM G150-13, "Standard Test Method for Electrochemical Critical Pitting Temperature Testing of Stainless Steels" (West Conshohocken, PA: ASTM International, 2013).

44. R. Johnsen, H. Vingsand, "Comparison of Corrosion Properties of UNS S32750, UNS N06022 and UNS N10276 in Seawater," EUROCORR 2008, paper no. 1089 (Edinburgh, U.K.: European Federation of Corrosion, 2008).

45. R. Johnsen, H. Vingsand, "Corrosion Properties of UNS S32750, UNS N06022 and UNS N10276 in Seawater," CORROSION 2009, paper no. 195 (Houston, TX: NACE, 2009).

46. ASTM A923-14, "Standard Test Methods for Detecting Detrimental Intermetallic Phase in Duplex Austenitic/Ferritic Stainless Steels" (West Conshohocken, PA: ASTM International, 2014).

47. ASTM A182/182M, "Standard Specification for Forged or Rolled Alloy and Stainless Steel Pipe Flanges, Forged Fittings, and Valves and Parts for High-Temperature Service" (West Conshohocken, PA: ASTM International, 2016).

48. ASTM G48-11, "Standard Test Methods for Pitting and Crevice Corrosion Resistance of Stainless Steels and Related Alloys by Use of Ferric Chloride Solution" (West Conshohocken, PA: ASTM International, 2011).

49. J.M. Pardal, S.S.M. Tavares, M.C. Fonseca, J.A. de Souza, R.R.A. Côrte, H.F.G. de Abreu, *Mater. Charact.* 60, 3 (2009): p. 165-172.

50. A.J. Sedriks, *Corrosion* 45, 6 (1989): p. 510-518.

51. S. Ronneteg, A. Juhlin, U. Kivisäkk, "Hydrogen Embrittlement Of Duplex Stainless Steels Testing of Different Product Forms at Low Temperature," CORROSION 2007, paper no. 498 (Houston, TX: NACE, 2007).

52. G. Lauvstad, R. Johnsen, I. Asbjørnsen, M. Bjurström, C.G. Hjorth, *Corrosion* 66, 11 (2010): p. 115004-1 to 115004-13.

53. G.S. Frankel, "Pitting Corrosion,"in *Corrosion Fundamentals, Testing, and Protection*, eds. S.D. Cramer, B.S. Covino Jr., ASM Handbook, vol. 13A (Materials Park, OH: ASM International, 2003), p. 236-241.

54. I. Betova, M. Bojinov, T. Laitinen, K. Mäkelä, P. Pohjanne, T. Saario, *Corros. Sci.* 44, 12 (2002): p. 2675-2697.

55. I. Betova, M. Bojinov, T. Laitinen, K. Mäkelä, P. Pohjanne, T. Saario, *Corros. Sci.* 44, 12 (2002): p. 2699-2723.

56. M. Næss, R. Johnsen, M. Iannuzzi, "Use of Electrochemical Techniques to Determine the Effect of Sigma (σ)-Phase Precipitation on a 25 wt% Cr Super Duplex Stainless Steel," CORROSION 2015, paper no. 5595 (Houston, TX: NACE, 2015).

57. B.S. DeForce, "Comments on ASTM G48 - Standard Test Methods for Pitting and Crevice Corrosion Resistance of Stainless Steels and Related Alloys by Use of Ferric Chloride Solution," CORROSION 2016 (Houston, TX: NACE, 2016).

58. R. Gundersen, B. Johansen, P.O. Gartland, L. Fiksdal, I. Vintermyr, R. Tunold, G. Hagen, *Corrosion* 47, 10 (1991): p. 800-807.

59. R. Francis, G. Byrne, G. Warburton, "The Corrosion of Superduplex Stainless Steel in Different Types of Seawater," CORROSION 2011, paper no. 351 (Houston, TX: NACE, 2011).

60. J.R. Galvele, *Corros. Sci.* 47, 12 (2005): p. 3053-3067.

61. L.F. Garfias-Mesias, J.M. Sykes, C.D.S. Tuck, *Corros. Sci.* 38, 8 (1996): p. 1319-1330.

62. D.H. Kang, H.W. Lee, *Corros. Sci.* 74 (2013): p. 396-407.

63. L.F. Garfias-Mesias, J.M. Sykes, *Corros. Sci.* 41, 5 (1999): p. 959-987.

64. L.F. Garfias-Mesias, J.M. Sykes, *Corrosion* 54, 1 (1998): p. 40-47.

65. R.A. Perren, T.A. Suter, P.J. Uggowitzer, L. Weber, R. Magdowski, H. Böhni, M.O. Speidel, *Corros. Sci.* 43, 4 (2001): p. 707-726.

66. "Outokumpu 2507 (UNS S32750)," Outokumpu High Performance Stainless, 2015.

67. "Sandvik SAF 2507 - (Tube and Pipe, Seamless)," Sandvik Materials Technology, 2016.

68. B. Deng, Y. Jiang, J. Gong, C. Zhong, J. Gao, J. Li, *Electrochim. Acta* 53, 16 (2008): p. 5220-5225.

69. T. Tsaprailis, I.W. Kovacs, J. Tuggle, L.F. Garfias-Mesias, "Corrosion Resistance of Stainless Steels Exposed to Aggressive Environments with Particles and Water," CORROSION 2009, paper no. 277 (Houston, TX: NACE, 2009).

70. T. Mathiesen, A. Anderko, "Challenges in Pre-Qualification Corrosion Testing of CRAs Based on ASTM G48," CORROSION 2014, paper no. 4272 (Houston, TX: NACE, 2014).

71. J.R. Galvele, *J. Electrochem. Soc.* 123, 4 (1976): p. 464.

72. N.J. Laycock, J. Stewart, R.C. Newman, *Corros. Sci.* 39, 10-11 (1997): p. 1791-1809.

73. J.B. Lumsden, Z. Szklarska-Smialowska, *Corrosion* 34, 5 (1978): p. 169-176.

74. "902 F No. 2511 - Corrosion Resistance of SM25CrW (DP3W) in Seawater Environment," Sumitomo Metal Industries Ltd., 902 F No. 2511, 1992.

75. "Alloy 6Mo (UNS S31254) Stainless Steel," Fine Tubes, 2011.

76. A.U. Malik, M. Mobin, F. Al-Muaili, S. Al-Forzan, "Corrosion Behavior of Duplex Stainless Steels in Arabian Seawater," CORROSION 2011, paper no. 171 (Houston, TX: NACE, 2011).

77. X. Shan, J.H. Payer, *Corrosion* 66, 10 (2010): p. 105005-1 to 105005-14.

78. M. Kappes, M. Rincón-Ortiz, M. Iannuzzi, R.M. Carranza, "Use of the Critical Acidification Model to Estimate Critical Localized Corrosion Potentials of Duplex Stainless Steels," CORROSION 2016, paper no. 7326 (Houston, TX: NACE, 2016).

79. P.A. Martínez, E.C. Hornus, M.A. Rodríguez, R.M. Carranza, R.B. Rebak, "Crevice Corrosion Resistance of Super-Austenitic and Super-Duplex Stainless Steels in Chloride Solutions," CORROSION 2015, paper no. 5740 (Houston, TX: NACE, 2015).

80. J.R. Galvele, J.B. Lumsden, R.W. Staehle, *J. Electrochem. Soc.* 125, 8 (1978): p. 1204.

81. M.R. Ortiz, M.A. Rodriguez, R.M. Carranza, R.B. Rebak, *Corrosion* 66, 10 (2010): p. 105002-1 to 105002-12.

82. M. Iannuzzi, C. Mendez, L. Avila-Gray, G. Maio, H. Rincon, *Corrosion* 66, 4 (2010): p. 045003-1 to 045003-8.

83. A.C. Lloyd, J.J. Noël, S. McIntyre, D.W. Shoesmith, *Electrochim. Acta* 49, 17-18 (2004): p. 3015-3027.

84. P. Jakupi, F. Wang, J.J. Noël, D.W. Shoesmith, *Corros. Sci.* 53, 5 (2011): p. 1670-1679.

85. A.K. Mishra, D.W. Shoesmith, *Corrosion* 70, 7 (2014): p. 721-730.

FIGURE 1. (a) and (b)Optical and (c) secondary electron images of solution annealed UNS S32750 showing an equiaxed fine grain structure characteristic of forged products, austenite (light) and ferrite (dark). Samples were free of deleterious intermetallic compounds and third phases. Specimens were etched in a 40 wt% NaOH solution using 1.5 V for 30 s to 40 s.

FIGURE 2. (a) and (b) Optical and (c) secondary electron images of solution annealed UNS S39274 showing elongated grains aligned in the rolling direction, characteristic of rolled plates, austenite (light) and ferrite (dark). Samples were free of deleterious intermetallic compounds and third phases. Specimens were etched in a 40 wt% NaOH solution using 1.5 V for 30 s to 40 s.

FIGURE 3. Cyclic anodic polarization curves of crevice-free UNS 39274 pickled samples exposed to 3.5 wt% NaCl, pH 8.0 showing: (a) no hysteresis loop, (b) small hysteresis, high E_P, and (c) clear positive hysteresis loop, temperature as indicated. The multiple anodic curves are replicate tests included to illustrate reproducibility.

FIGURE 4. (a) E_{Trans} or E_P and (b) E_{Trans} or E_{RP} vs. temperature for crevice-free UNS S39274 with pickled surfaces. Lines added to aid visualization. Each data point represents an average of two or three independent CPP tests.

FIGURE 5. CCT|E_{RP} comparison between crevice-free UNS S32750 and UNS S39274 pickled samples showing the direct effect of W on localized corrosion resistance. Lines added to aid visualization. Each data point represents an average of two or three independent CPP tests.

FIGURE 6. (a) E_{Trans} or E_{Crev} and (b) E_{Trans} or $E_{RP, Crev}$ vs. temperature for creviced UNS S32750 or S39274 pickled surfaces as indicated. Lines added to aid visualization. Each data point represents an average of two or three independent CPP tests.

FIGURE 7. Electrochemical CPT of crevice-free UNS S32750 and UNS S39274 (pickled) as indicated determined in accordance with ASTM G150 at an applied anodic potential of E_{App} = +600 mV_{SCE}.

FIGURE 8. E_{corr} vs. time for creviced (a) UNS S32750 and (b) UNS S39274 (pickled)in filtered natural seawater. The image inserts show the surface condition after testing. Whereas UNS S32750 suffered crevice corrosion at 60°C, UNS S39274 was tested up to 80°C, temperature steps as indicated. Crevice corrosion was found close to the edge of the crevice formers.

FIGURE 9. Secondary electron images of (a) and (b) UNS S32750 and (c) and (d) UNS S39274 creviced samples after long-term OCP exposure in natural seawater, illustrating crevice corrosion attack close to the open surface//crevice former boundary. Clear preferential dissolution of the austenite phase was observed in UNS S32750. Preferential dissolution was not evident in the high-W UNS S39274 samples. The depth of the crevice corrosion attack was shallower on UNS S39274 than on S32750, even though the high-W grade was exposed up to 80°C for over 1,700 h.

Table 1 Nominal Composition of Typical DSS and SDSS[47]

UNS	Cr (wt%)	Mo (wt%)	Ni (wt%)	N (wt%)	Other (wt%)
S32205	22 to 23	3.0 to 3.5	4.5 to 5.6	0.14 to 0.20	Mn<1.2, S<0.001, P<0.030, C< 0.020, Si<0.8
S32750	24 to 26	3.0 to 5.0	6.0 to 8.0	0.24 to 0.32	Mn<1.2, S<0.015, P<0.035, C< 0.030, Si<0.8
S32550	24 to 27	2.9 to 3.9	4.5 to 6.5	0.10 to 0.25	Cu:1.50-2.50, Mn< 1.5, S <0.03, P<0.04, C< 0.030, Si<1.0
S32760	24 to 26	3.0 to 4.0	6.0 to 8.0	0.20 to 0.30	W: 0.5-1.0, Cu: 0.5-1.0, Mn<1.0, S<0.01, P<0.03, C<0.030, Si<1.0

Table 2 Mechanical Properties and CPT and CCT of Conventional Stainless Steels and Nickel Alloys[66-67,75]

Property	22Cr DSS	25Cr SDSS	UNS S31603	UNS S31254	UNS N06625	UNS N07725
SMYS or R_P (0.2% offset) (MPa)	450	550	205	310	415	920
Tensile Strength, R_M (MPa)	620	750	515	675	825	1,268
Min. Elongation to Failure, A (%)	25	25	35	35	30	30

Table 3 Actual Chemical Composition in wt% and PRE

UNS	C	Si	Mn	P	S	Cr	Mo	Ni	W	Cu	N	Co	PRE_N	$PRE_{N,W}$
S32750	0.02	0.32	0.56	0.019	0.0004	25.74	3.31	6.92	0.55	0.20	0.267	<0.05	40.93	41.84
S39274	0.016	0.20	0.80	0.045	0.003	25.2	3.20	6.40	2.20	0.52	0.28	-	40.24	43.87

Table 4 Actual Mechanical Properties of Tested Materials

UNS	$R_{P\ 0.2}$ (MPa)	R_M (MPa)	Elongation to failure, A (%)	Avg. CVN (J) at 46°C	Hardness (HRC)
S32750	582	830	38	305.7	22.5
S39274	611	880	41	119	25.5

Table 5 Summary of CPT and CCT Values as Determined by CPP or ASTM G150 as Indicated

Microstructure	Surface Finish	CPT (°C), ASTM G61		Mean T_{Prot} or CCT|E_{RP} (°C) ASTM G61	CPT (°C), ASTM G150	
		min.	max.		min.	max.
UNS S32750	Polished (600 grit SiC)	65	75	55	-	-
UNS S32750	Pickled (NORSOK M-630)	75	75	55	63.5	65.2
UNS S39274	Polished (600 grit SiC)	85	85	80	-	-
UNS S39274	Pickled (NORSOK M-630)	85	85	85	95	>99

Table 6 Summary of CCRT Values as Determined by CPP

UNS	Surface Finish	CCRT (°C)		Mean CCRT (°C)
		min.	max.	
S32750	Pickled and passivated	55	60	57.5
S39274	Pickled and passivated	65	70	67.5

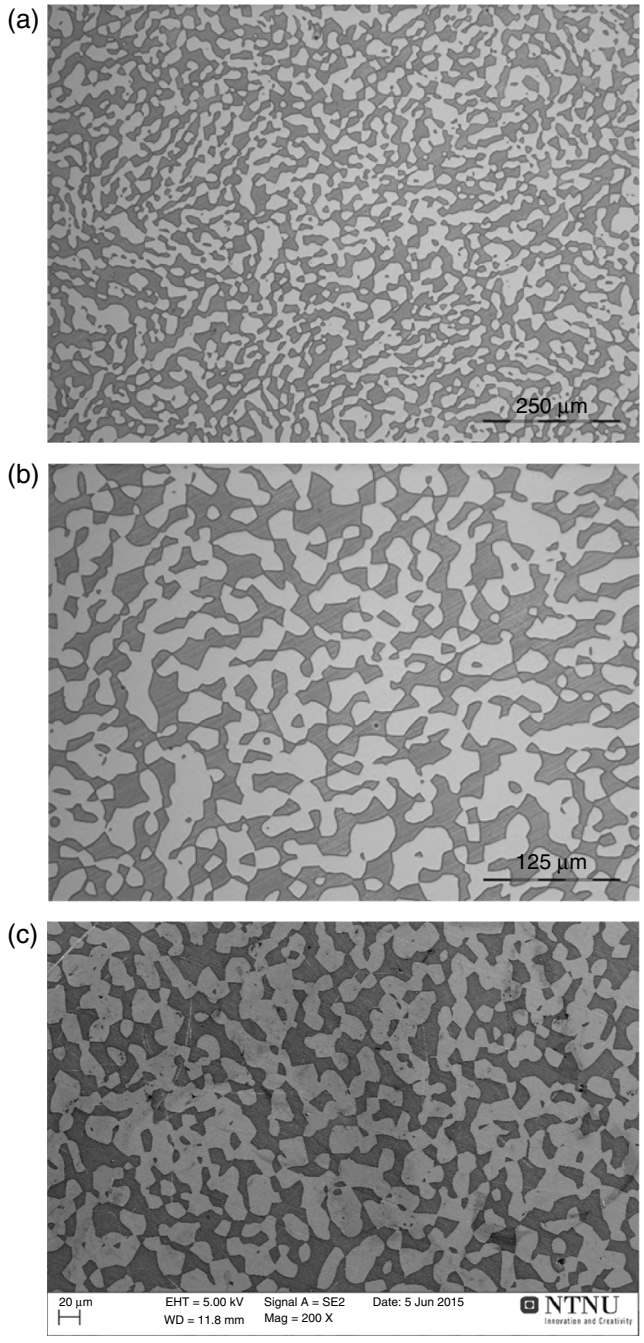
(a)
250 µm
(b)
125 µm
(c)
20 µm
EHT = 5.00 kV
WD = 11.8 mm
Signal A = SE2
Mag = 200 X
Date: 5 Jun 2015
NTNU
Innovation and Creativity

FIGURE 1.

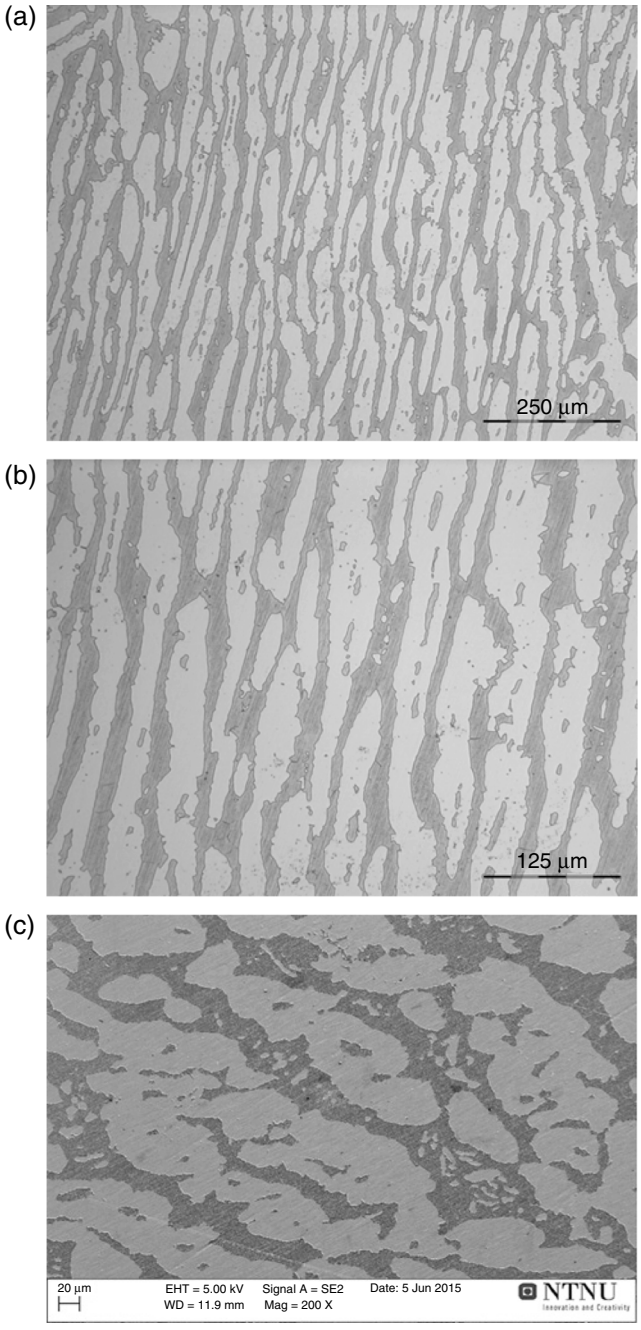
(a)
250 µm
(b)
125 µm
(c)
20 µm
EHT = 5.00 kV
WD = 11.9 mm
Signal A = SE2
Mag = 200 X
Date: 5 Jun 2015
NTNU
Innovation and Creativity

FIGURE 2.

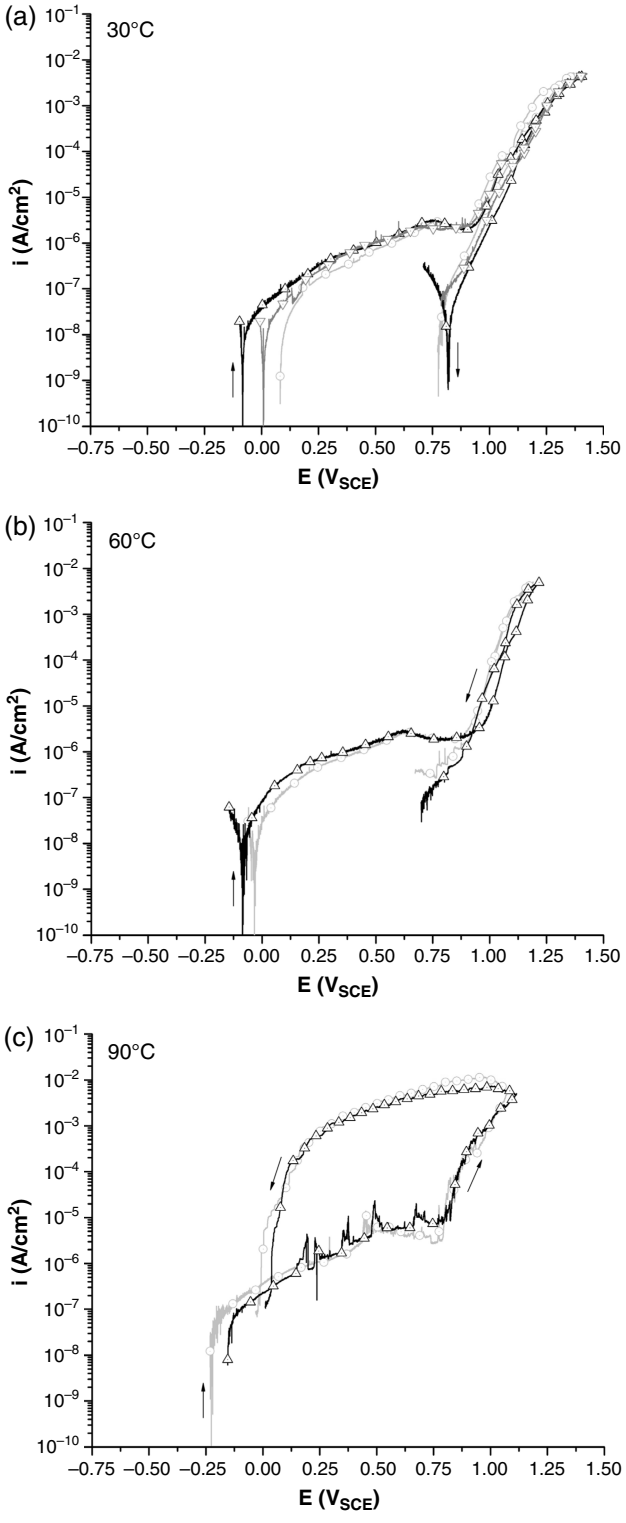
(a)
30°C
(b)
60°C
(c)
90°C
i (A/cm²)
E (V_SCE)
10⁻¹
10⁻²
10⁻³
10⁻⁴
10⁻⁵
10⁻⁶
10⁻⁷
10⁻⁸
10⁻⁹
10⁻¹⁰
−0.75 −0.50 −0.25 0.00 0.25 0.50 0.75 1.00 1.25 1.50

FIGURE 3.

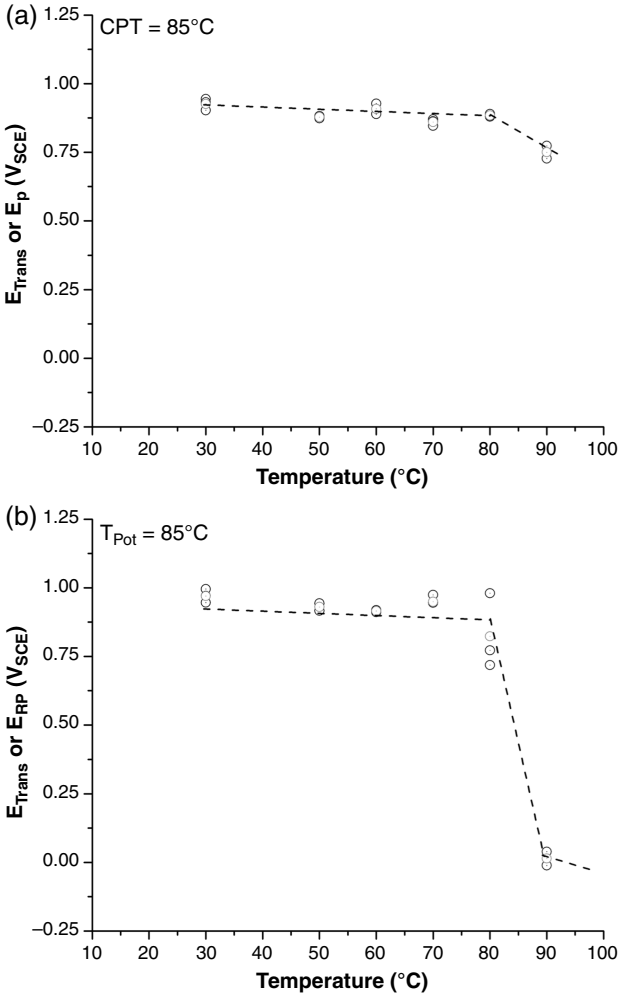

FIGURE 4.

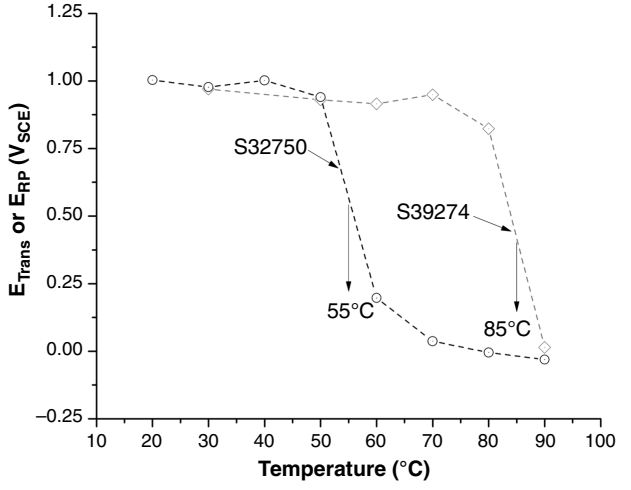

FIGURE 5.

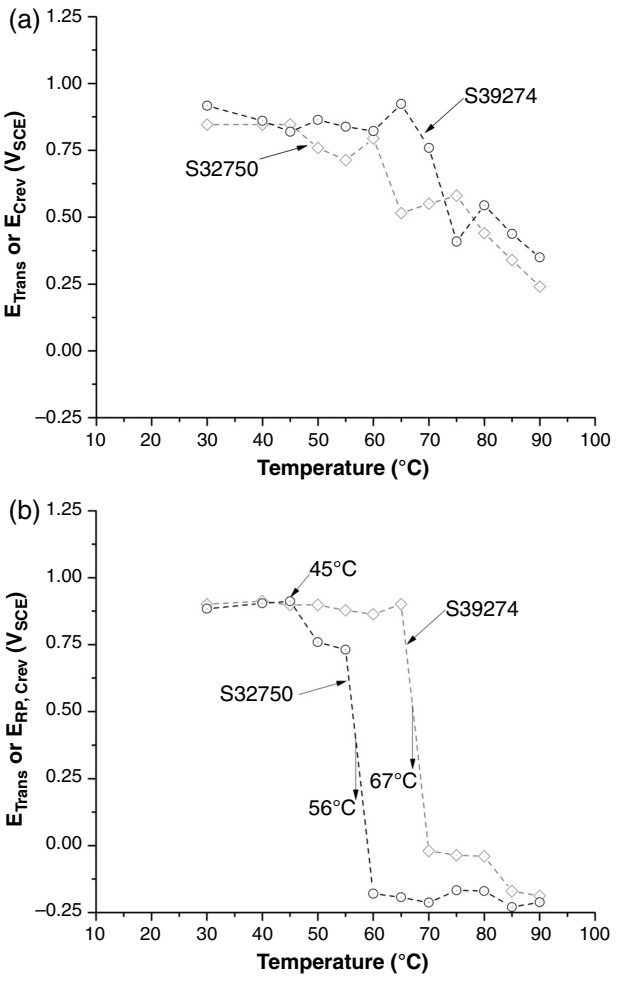

FIGURE 6.

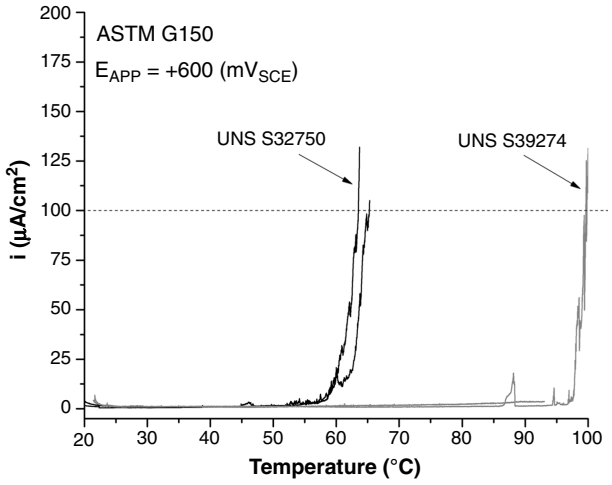

FIGURE 7.

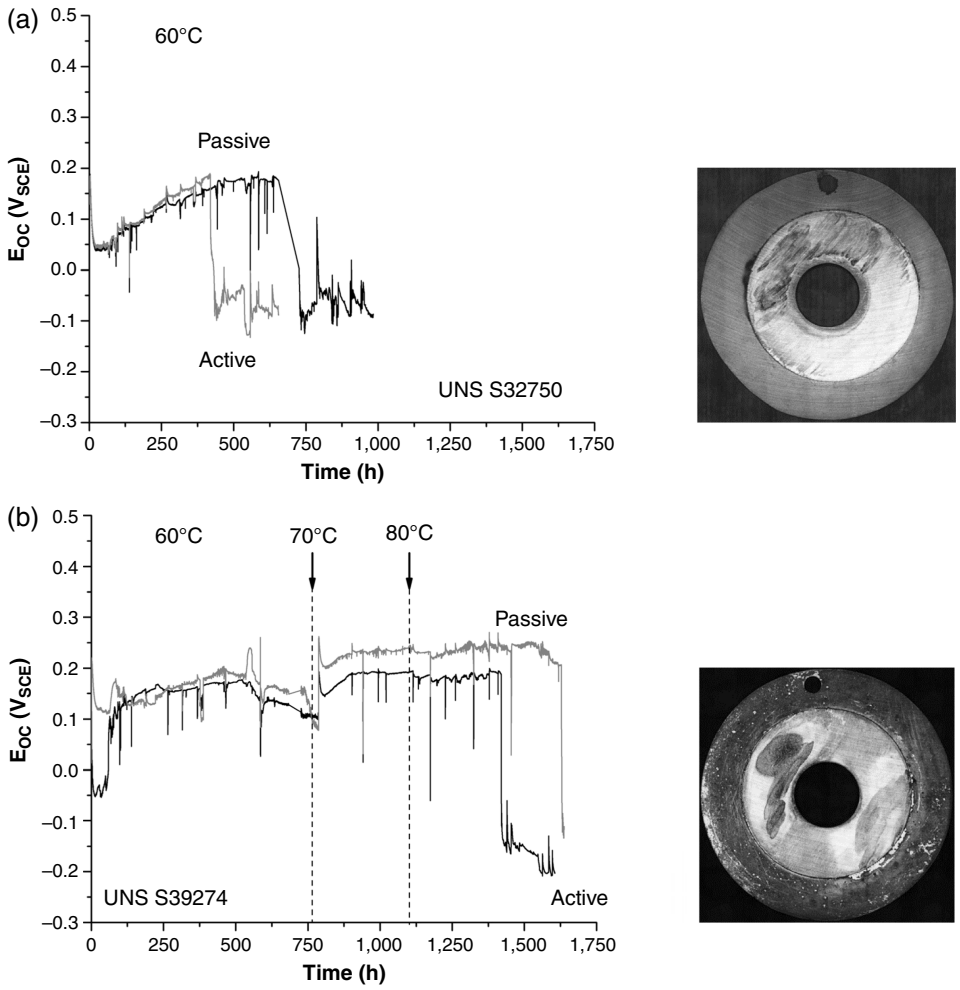
(a)
60°C
Passive
Active
UNS S32750
E_{OC} (V_{SCE})
Time (h)
(b)
60°C
70°C
80°C
Passive
UNS S39274
Active
E_{OC} (V_{SCE})
Time (h)

FIGURE 8.

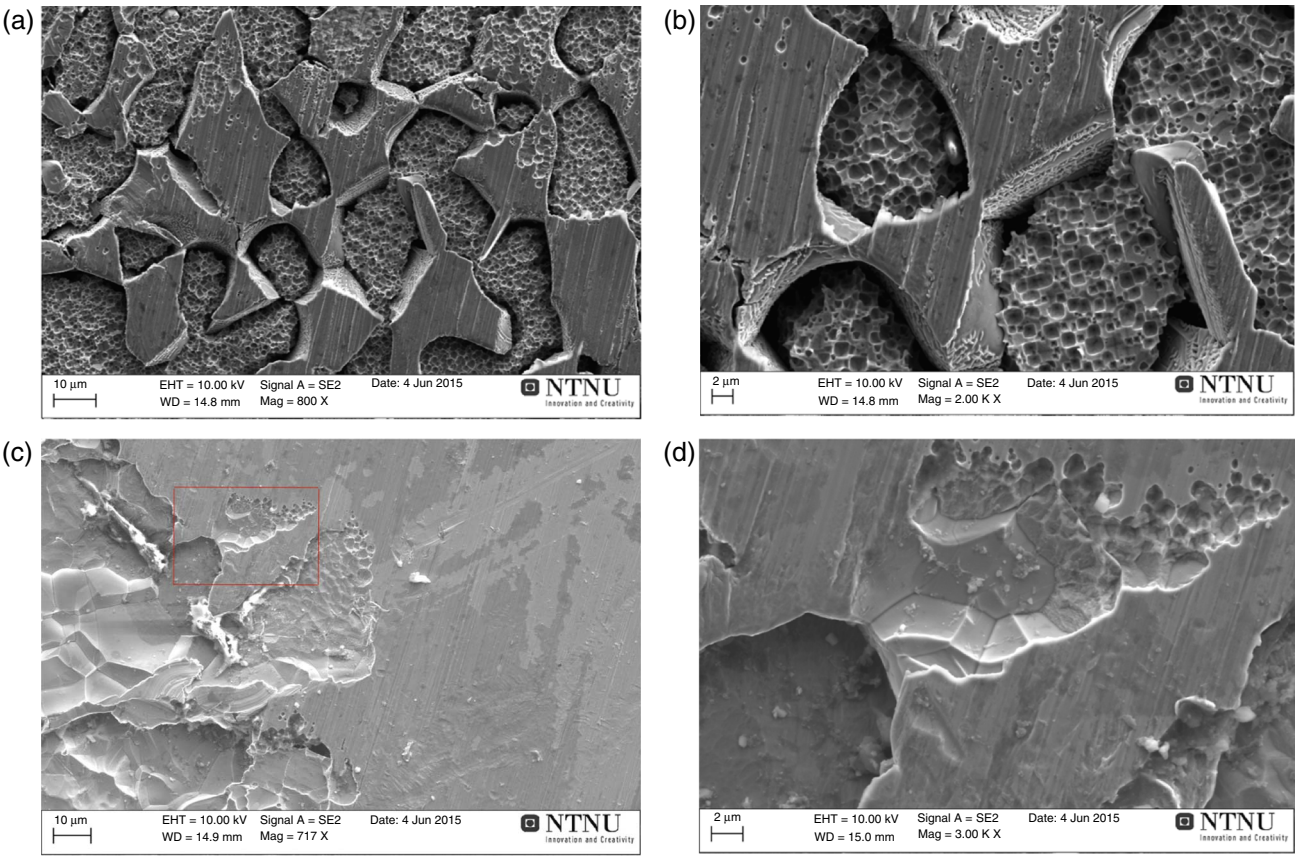
(a)
10 µm
EHT = 10.00 kV
WD = 14.8 mm
Signal A = SE2
Mag = 800 X
Date: 4 Jun 2015
NTNU
Innovation and Creativity
(b)
2 µm
EHT = 10.00 kV
WD = 14.8 mm
Signal A = SE2
Mag = 2.00 K X
Date: 4 Jun 2015
NTNU
Innovation and Creativity
(c)
10 µm
EHT = 10.00 kV
WD = 14.9 mm
Signal A = SE2
Mag = 717 X
Date: 4 Jun 2015
NTNU
Innovation and Creativity
(d)
2 µm
EHT = 10.00 kV
WD = 15.0 mm
Signal A = SE2
Mag = 3.00 K X
Date: 4 Jun 2015
NTNU
Innovation and Creativity

FIGURE 9.